Steady Shear Flow Alignment and Rheology of Lamellae-Forming ABC Triblock Copolymer Solutions: Orientation, Defects, and Disorder

Emanuela Di Cola,[†,‡] Carine Fleury,[†] Pierre Panine,[‡] and Michel Cloitre*[,†]

Laboratoire Matière Molle et Chimie, UMR ESPCI-CNRS 7167, ESPCI, 10 rue Vauquelin, 75231 Paris, France, and European Synchroton Research Facility, 6 rue Jules Horowitz, 38043 Grenoble, France

Received December 27, 2007; Revised Manuscript Received March 7, 2008

ABSTRACT: The effect of steady shear flow on the morphology and rheology of two lamellae-forming polystyrene-*block*-polybutadiene-*block*-poly(methyl methacrylate) copolymer solutions has been studied using time-resolved Rheo-SAXS experiments. The main effect of shear flow is to reversibly align the ordered lamellae in perpendicular orientation with long-range order at low shear rates and in parallel orientation at high shear rates. The crossover from low to high shear rates behavior occurs at $\dot{\gamma}_c \approx \tau^{-1}$, where τ is the single chain relaxation time. Both orientations coexist in the vicinity of $\dot{\gamma}_c$ without any apparent drift toward a well-defined state. Whereas a high degree of perpendicular alignment is achieved at low shear rates, the parallel alignment above $\dot{\gamma}_c$ is highly defective, and it is progressively destroyed by the flow. Upon flow cessation, the fraction of disordered material rearranges into lamellae in transverse alignment. These results highlight the specificity of strong shear flows with respect to oscillatory shear flows commonly used to align block copolymers and of ABC mesophases with respect to other block copolymers mesophases.

I. Introduction

Block copolymers exhibit complex dynamics when subjected to external mechanical fields. Shear flows can cause microphase-separated block copolymers to align in large domains with long-range translational order and various orientations depending on the experimental conditions. The behavior of block copolymers under flow is fundamental to the design and the processing of these materials. When a high degree of flow alignment can be achieved, it is possible to fabricate highly organized anisotropic materials with interesting properties that have numerous potential applications in conventional and advanced technologies. Moreover, since the resistance to flow strongly depends on the orientation of the microstructure with respect to the axis of deformation, the coupling between flow and microstructure greatly influences the linear and nonlinear rheology of block copolymers.

In past years the behavior of lamellar block copolymers has stimulated a lot of work. Many studies have focused on diblock copolymer melts under large-amplitude oscillatory shear flows. Two main orientations have been identified: (1) the perpendicular orientation where the normal to the lamellae is oriented along the shear gradient (Figure 1a); (2) the parallel orientation where the normal is along the vorticity direction (Figure 1b). The selection of one particular orientation depends primarily on the frequency ω of the oscillatory strain. Three frequency regimes have been identified and conceptualized.[1−5] These regimes are separated by the characteristic frequencies ω_d and ω_c. ω_c is of the order of the inverse of a single chain relaxation time. ω_d is a characteristic frequency associated with the relaxation of defects between microdomains. In the low- and high-frequency regimes ($\omega < \omega_d$ and $\omega > \omega_c$), shearing leads to parallel orientation, whereas in the intermediate frequency regime ($\omega_d < \omega < \omega_c$) the shear stable alignment is perpendicular. A third possible orientation, the transverse orientation where the normal is oriented along the velocity direction (Figure 1c), has been reported. It generally occurs in combination with other orientations during transient states[5−7] and/or in the presence of specific defects like kink bands.[8,9] In one situation, where the chain dynamics was dominated by the presence of entanglements, pure transverse alignment has been reported.[10]

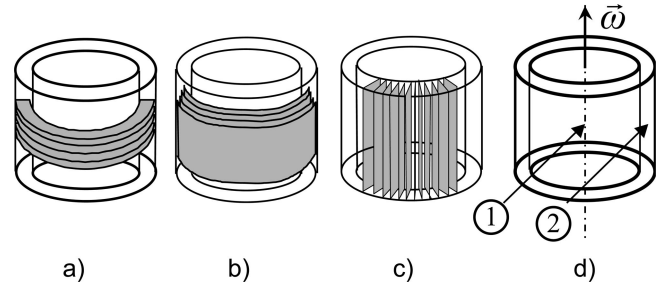

Figure 1. Three possible states of macroscopic alignment of lamellae under shear flow in a Couette cell. The velocity direction ($\vec{V}$) and the shear gradient direction ($\vec{\nabla V}$) are parallel and normal to the walls, respectively; the vorticity ($\vec{\omega}$) direction is along the axis of rotation. (a) Perpendicular alignment: the layers are perpendicular to the walls. (b) Parallel alignment: the layers are parallel to the walls. (c) Transverse direction: the normal to the layers is along the velocity direction. (d) Relative arrangement of the SAXS beam and of the Couette cell showing the radial (1) and tangential configurations (2).

For a given diblock copolymer not all orientations are systematically observed. Experimentally, the selection of a particular state of orientation is a complex process that involves the interplay of many parameters. Chain distortions and molecular relaxations play a central role in the development of parallel alignment at high frequencies.[11] A large contrast in the viscoelastic properties of the blocks also favors the parallel orientation since in it the strain is localized in the softer blocks, which lowers the overall stress.[1,3,12] The thermomechanical history of the copolymer also plays an important role. Parallel orientation is achieved at low frequency only when the melt is annealed at temperature below the order−disorder temperature (T_{ODT}) before shearing.[13] In the same vein, shearing as the melt is cooled from above T_{ODT} systematically leads to uniform perpendicular alignment, while parallel alignment is preferred

* Corresponding author: e-mail michel.cloitre@espci.fr.
† UMR ESPCI-CNRS 7167.
‡ European Synchroton Research Facility.

10.1021/ma702876k CCC: $40.75
Published on Web 04/25/2008

when the shearing is applied once in the ordered state.[1] The proximity of the temperature to T_{ODT} is then another crucial parameter.[1,5,14] The processing steps prior to shear application can also induce a particular orientation and/or specific trapped defects that will greatly influence the outcome of subsequent shearing experiments.[9] Finally, the strain amplitude not only influences the rate and the degree of alignment but also contributes to the selection of the direction of alignment.[5,15,16]

Fewer studies have investigated the alignment of diblock copolymer solutions under reciprocating shear flow.[17–20] The results are globally consistent with the behavior of melts, except that parallel alignment is never observed at very low frequencies.

Notwithstanding the conceptual importance of diblock copolymers, practical applications of block copolymers rely on triblock or multiblock molecular architectures, which involve bridging and looping of the internal blocks. The most comprehensive studies of flow alignment of multiblock copolymers have focused on ABA triblock and ABABA pentablock copolymer melts.[14,21–24] Although triblock copolymers share common features with diblocks, they exhibit a greater sensitivity to experimental conditions, and several contradictory results have been reported.[14,21–23] In pentablock copolymers,[24] the only stable arrangement is the low-frequency perpendicular orientation. A transition to a disordered state occurs at high frequency. Upon flow cessation, the molecules reorder into a well-defined stable transverse orientation. This behavior has been interpreted in relation with the pentablock architecture that imposes a strong mechanical coupling between the block layers and prevents the microdomains from sliding relative to each other, thus destroying the parallel orientation.[24] Similar arguments have been developed for other multiblock copolymers.[25]

While all these studies have focused on flow alignment dynamics of block copolymer melts subjected to reciprocating shear flows at fixed amplitude, comparatively little attention has been paid to block copolymers in steady shear flow. Yet steady flows are commonly involved in engineering processes used to process films, fibers, and coatings. For instance, copolymer solutions roll-casting has proved to be a reliable method to produce films with long-range order.[26] In addition, given that the strain amplitude and the frequency have appeared to be important parameters in oscillatory flow alignment, new phenomena are expected to occur in strong flow conditions where large strains accumulate during shearing. It has been found that the orientation in diblock solutions flips from perpendicular to parallel when the shear rate is increased but that the parallel alignment at high shear rates is associated with highly nonlinear elasticity.[20] For the case of extrusion, it has been reported that diblock copolymers orient in parallel and perpendicular directions or become disordered depending on the shear rate and on annealing.[27,28] Still more puzzling, the extrusion of pentablock solutions at high shear rates produces a stable transverse orientation at high shear rates.[29]

In this paper, we investigate the alignment of lamellae forming ABC copolymer solutions under steady shear flow and the relation with the rheological properties. ABC copolymers have a higher degree of complexity than AB and ABA copolymers due to their connectivity. In ABC copolymers the midblocks B necessarily bridge the end blocks A and C, which belong to two different microdomains. By contrast, in ABA copolymers the midblocks can adopt a loop or a bridge conformation so that they belong either to the same or to different microdomains. Another characteristic feature of this work is that it focuses on solutions with very low viscosity where the molecular relaxation time of block copolymer chains (~0.1 s) is much shorter than the typical duration of an experiment, allowing us to avoid long-lived intermediate states that may arise from slow chain or domain relaxation. One additional motivation to study the flow properties of block copolymer solutions is their major impact on the recovery processes that follow the synthesis of these materials.

Table 1. Properties of the Two Block Copolymers $S_xB_yM_z$ Used in This Study[a]

copolymer	x	y	z	f_S	f_B	f_M	M_w	PDI
$S_{11}B_{19}M_{70}$	0.11	0.19	0.70	0.11	0.24	0.65	216 450	1.5
$S_{24}B_{21}M_{55}$	0.24	0.21	0.55	0.24	0.26	0.50	148 625	1.2

[a] Subscripts x, y, and z refer to the weight fraction of the components S, B, and M. f_i designate the volume fraction of block i. M_w is the weight-average molar mass. The index of polydispersity (PDI = M_w/M_n, where M_n is the number-average molar mass) is for the entire triblock copolymers.

The ABC copolymers studied in the following are polystyrene (S)-*block*-polybutadiene (B)-*block*-poly(methyl methacrylate) (M), designated as SBM hereafter. When dissolved in weakly selective solvents, SBM copolymers self-assemble into mesophases with various morphologies. Here we focus on two different SBM compositions leading to lamellar mesophases. One is an asymmetric copolymer that forms two-phase lamellae when the end blocks segregate into mixed S + M microdomains. The second one is a symmetric copolymer that self-assembles into three-phase lamellae with the end blocks laying into distinct microdomains. The first copolymer is similar to a ABA copolymer while the second one exhibits the typical behavior of true ABC copolymers. We simultaneously probe the degree of order, the state of orientation, and the associated rheological properties of mesophases using time-resolved Rheo-SAXS experiments. Two main orientations are found: a perpendicular orientation at low shear rates and a highly defective parallel orientation at shear rates just above the inverse of the relaxation time of individual chains. The lamellar alignment reversibly flips from one orientation to another. At much higher shear rates, a significant fraction of lamellae is destroyed by the flow and reorient in transverse orientation upon flow cessation. These phenomena are associated with peculiar variations of the viscosity with the shear rate.

II. Experimental Section

II.1. Materials and Sample Preparation. The poly(styrene-*block*-butadiene-*block*-methyl methacrylate) triblock copolymers (SBM) used in this study were synthesized by anionic polymerization by Arkema using procedures described elsewhere.[30] The as-received powder is a mixture of poly(styrene-*block*-butadiene) diblock copolymer (SB) and of SBM triblock copolymer. The SB diblocks were extracted as follows.[31] The powder was first dispersed in a mixture of cyclohexane and *n*-heptane (60/40 wt %), which is a selective solvent for SB diblocks. The dispersion was then heated at 84 °C for 2 h under vigorous stirring. At the end of the extraction, the dispersion was centrifuged, and the supernatant was carefully removed. The solid part, which mainly contains SBM triblocks, was rinsed with the cyclohexane/*n*-heptane mixture and dried under vacuum. The selectivity and the efficiency of the extraction were checked by size exclusion chromatography (SEC) and ^{1}H NMR. The process was repeated several times to achieve a high degree of purity. The product obtained after three successive operations contained less than 1 wt % of SB. The composition and the polydispersity of the S and M blocks were analyzed by SEC after selective ozonolysis of the B blocks. The S and M blocks were found to have the same polydispersity index (PDI ≅ 1.2), yielding a total polydispersity index of the order of 1.4. To characterize the copolymers, we use the $S_xB_yM_z$ nomenclature, where the subscripts x, y, and z refer to the weight fraction of the components. The characteristics of the two SBM copolymers used in this study are listed in Table 1.

Solutions of SBM copolymers were prepared by dissolving the required amount of polymer in toluene, which is a good solvent for each block of the copolymer. Solutions were carefully stirred

during at least 48 h to ensure complete dissolution and homogeneity. The copolymer concentration was expressed in terms of the weight fraction of copolymer hereafter denoted by C (g/g). C was systematically varied between 0.05 and 0.30 g/g in increments of 0.05 g/g.

II.2. Rheometry. A Haake RS150 rheometer was used for rheological experiments. For laboratory measurements, the rheometer was equipped with a cone and plate geometry (35 mm in diameter; 2° angle). A solvent trap was especially designed to reduce solvent evaporation during long duration measurements. Calibration and testing of the system have shown that evaporation does not affect measurements up to 15 000 s. For combined SAXS and rheometry investigations, we used a homemade aluminum Couette cell. Solvent evaporation was minimized using a cap attached to the rotor. This allowed us to work for at least 4 h without any significant change in the rheological properties. The radius of the inner cylinder (rotor) was 10 mm. The gap between the rotor and the stator was 1 mm. We first determined the domain of linear viscoelasticity by performing dynamic stress sweeps at a frequency of 1 Hz. In practice, the strain response was linear in stress when the strain amplitude did not exceed the value $\gamma_0 \cong 0.01$. All dynamic measurements were performed in this linear viscoelasticity domain in order to preserve the structure of the solutions. Flow alignment experiments in steady shear flow were performed by applying a constant stress and recording the time evolution of the strain and of the shear rate until steady state was reached. It is important to note that since the order transition was not accessible even at moderate concentration, annealing was not possible and the shear flow was systematically applied on an ordered phase.

II.3. Rheo-SAXS. Small-angle X-ray scattering (SAXS) experiments under shear flow were performed on the High Brilliance beamline ID02 at the ESRF (Grenoble, France). The optics was used at a fixed wavelength of $\lambda = 0.1$ nm. The sample-to-detector distance was set at a distance of 10 m. The scattering vectors q accessible with the setup are in the range [0.015 nm^{-1}, 0.568 nm^{-1}] ($q = 4\pi \sin(\theta/2)/\lambda$ where θ is the scattering angle). The experimental resolution was $\Delta q = 0.0075$ nm^{-1}. The shape and the size of the beam (300 μm) were controlled by two orthogonal rectangular slits. The rheometer was mounted on a motorized translation stage, which allowed accurate positioning in the horizontal and vertical planes relative to the incident beam. We used two experimental configurations that are illustrated in Figure 1d: the radial configuration where the beam intersects the axis of symmetry of the Couette cell and the tangential configuration where the beam passes through the edge of the cell. For both cases, perfect alignment of the beam direction with respect to the cell is crucial. In the radial configuration, the beam is parallel to the velocity-gradient direction, and we detect the scattering patterns in the flow−vorticity plane ($\vec{q}_{\vec{v}}, \vec{q}_{\vec{\omega}}$) ($\vec{\omega}$ is the vorticity direction). In the tangential configuration, the beam is parallel to the velocity direction, and we obtain the scattering patterns in the shear gradient−vorticity plane ($\vec{q}_{\vec{\nabla v}}, \vec{q}_{\vec{\omega}}$). Because of the high flux available on the beamline and to the high electron density contrast between the blocks, the time of integration per image was as low as 20 ms, allowing us to perform time-resolved experiments.

Two-dimensional spectra were collected by a Thomson X-ray image intensifier optically coupled to a CCD-based FReLoN detector (fast read-out and low-noise detector). Raw images were converted to absolute intensities using the scattering from a Lupolen standard.[32] We took the path lengths in the radial and tangential configurations equal to 2 and 6.5 mm, respectively. Normalized images were corrected from the background scattering by subtracting the pattern scattered by the Couette cell filled with toluene. The resulting scattering patterns were analyzed in two different ways. First, we reduced the two-dimensional images to one-dimensional spectra $I(q)$ by integrating the intensity over the azimuthal angle Φ. The origin of the azimuthal angle coincides with the horizontal $\vec{q}_{\vec{v}}$ and $\vec{q}_{\vec{\nabla v}}$ axes, respectively, for the radial and tangential configurations. Second, we extracted the azimuthal dependence of the intensity at the principal peak wave vector (q^*) by integrating the intensity over a circular ring of width $\delta q = 2.5 \times 10^{-3}$ nm^{-1} centered on q^*. The plots showing the variations of $I(\Phi)$ vs Φ are called azimuthal plots in the following.

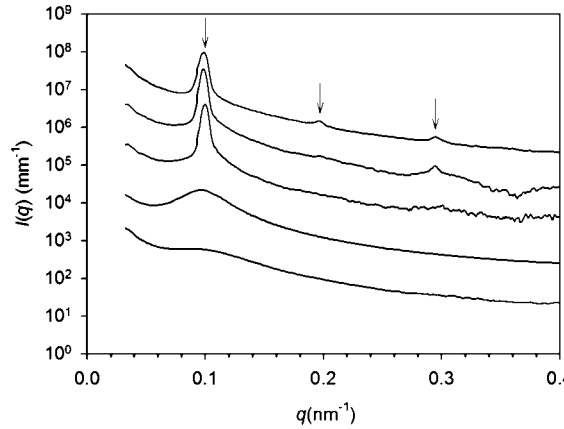

Figure 2. SAXS intensity vs scattering vector from solutions of $S_{11}B_{19}M_{70}$ in toluene at different concentrations (from bottom to top: $C = 0.10$, 0.15, 0.20, 0.25, and 0.30 g/g). For clarity, the data for $C =$ 0.15, 0.20, 0.25, and 0.30 g/g are shifted upward by 1, 2, 3, and 4 decades, respectively. For $C \geq 0.25$ g/g three orders of diffraction are visible (shown by arrows).

III. Results

III.1. Ordering Transition vs Concentration. The two-dimensional SAXS patterns of quiescent solutions exhibit isotropic diffraction rings allowing us to calculate scattering profiles $I(q)$ by radial integration over the azimuthal angle. Figure 2 presents the scattering profiles of $S_{11}B_{19}M_{70}$/toluene solutions at different concentrations ranging from $C = 0.05$ g/g to $C = 0.30$ g/g. The scattering intensity increases significantly, and the shape of the peak changes drastically when the concentration is increased. For $C \leq 0.15$ g/g, the peak intensity is low and the peak width is large. This broad peak indicates that the copolymer solution is fully disordered. For $C \geq 0.20$ g/g, the Bragg peaks become sharp and intense. At the largest concentrations investigated, higher order diffraction peaks are observed. These results show that solutions of $S_{11}B_{19}M_{70}$ in toluene exhibit a transition from a disordered state to an ordered state at a relatively low concentration.

Figure 3 shows that the linear viscoelastic properties of the solutions also change drastically at the transition. For $C = 0.175$ g/g, the elastic $G'(\omega)$ and viscous $G''(\omega)$ modulus vary much like in a disordered polymer solution. At low frequency, terminal behavior is observed with $G'(\omega) \sim \omega^2$ and $G''(\omega) \sim \omega$. The characteristic relaxation time of individual chains can be estimated from the limit $(G'/\omega G'')_{\omega \to 0}$ or similarly from the frequency at which $[G'(\omega)]_{\omega \to 0}$ crosses $[G''(\omega)]_{\omega \to 0}$. From the data shown in Figure 3 we deduce that $\tau \sim 0.1$ s at 20 °C. For $C = 0.25$ g/g, G' and $G''(\omega)$ are nearly equal and follow a power law variation with an exponent of about 0.5: $G'(\omega) \sim G''(\omega) \sim \omega^{0.5}$. This is the characteristic behavior expected for multigrain lamellar materials.[33]

We have determined the transition between the disordered state and the microphase-separated state from (a) the variations of the maximum peak intensity (I_{max}) and of the width of the peak at half-maximum (δq) with the concentration and (b) from the increase of the shear modulus with concentration (Figure 4). I_{max} exhibits a sharp drop, and δq decreases by more than 1 order of magnitude near $C = 0.175$ g/g. The storage modulus rises sharply around $C = 0.18$ g/g. In conclusion, ordering in $S_{11}B_{19}M_{70}$/toluene solutions occurs in the narrow range of concentrations (0.175 g/g $< C <$ 0.18 g/g).

Similar behavior was observed for the solutions of $S_{24}B_{21}M_{55}$ in toluene. They exhibit a disorder−order transition as the

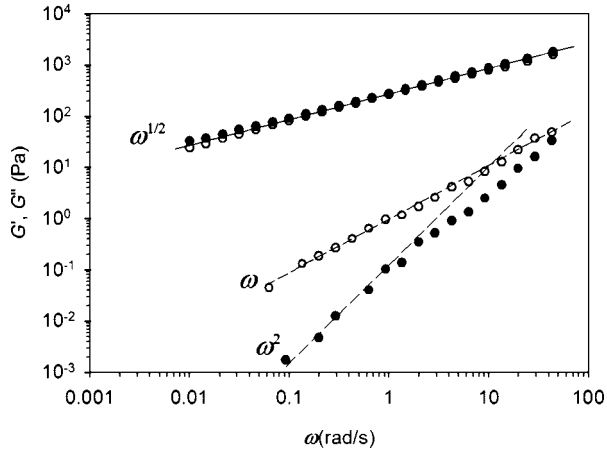

Figure 3. Linear viscoelastic properties of solutions of $S_{11}B_{19}M_{70}$ in toluene below and above the ordering concentration (storage modulus, G': full symbols; loss modulus, G'': open symbols). The top curves are for an ordered solution at $C = 0.25$ g/g. The bottom curves are measured for a disordered solution at $C = 0.175$ g/g. The dashed lines show that the disordered solution exhibits a terminal behavior; from their intersection (shown by the arrow), we estimate the characteristic relaxation time of the chains.

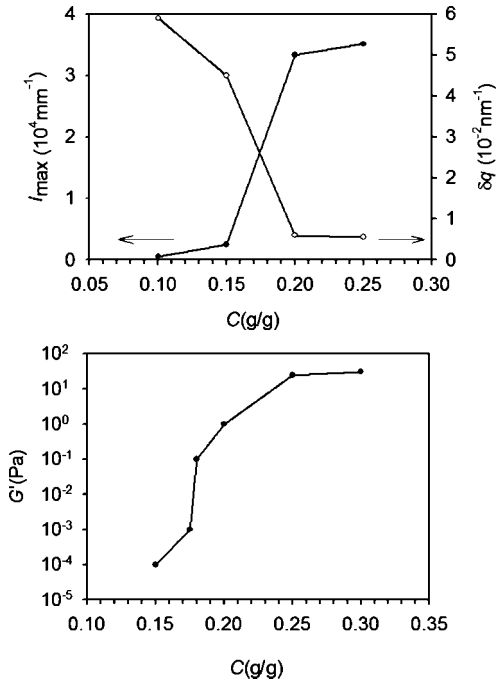

Figure 4. Determination of the ordering concentration of $S_{11}B_{19}M_{70}$ in toluene. Top: variations of the maximum peak intensity (I_{max}) and of the peak width measured at half-maximum (δq) vs polymer concentration. Bottom: variations of the shear modulus measured at $\omega = 0.1$ rad/s vs polymer concentration.

copolymer concentration is increased. The value of the ordering concentration ($C \cong 0.2$ g/g) is slightly larger than that found previously in $S_{11}B_{19}M_{70}$/toluene solutions, which is due to the lower molecular weight of $S_{24}B_{21}M_{55}$. The characteristic relation of the chains measured in the disordered state is very close to that found for the $S_{11}B_{19}M_{70}$ ($\tau \sim 0.05$ s).

III.2. Structure of Solutions in the Ordered State. In Figure 2, we observe that the positions of the maxima of the higher order scattering peaks are integer multiples of the position of the first-order peak ($q_m = 0.0994$ nm^{-1}). This shows that $S_{11}B_{19}M_{70}$/toluene solutions have a lamellar morphology with a long period $d_m = 63.2$ nm for a volume fraction $\phi = 0.25$. The scattering profiles of $S_{24}B_{21}M_{55}$/toluene solutions (not shown) also reveal lamellar morphology with a long period $d_m = 94.1$ nm when $\phi = 0.26$. Clearly, the long period of $S_{11}B_{19}M_{70}$/toluene lamellar mesophases is much smaller than the long period of $S_{24}B_{21}M_{55}$/toluene solutions even though the degree of polymerization of $S_{11}B_{19}M_{70}$ ($N = 1655$) is larger than that of $S_{24}B_{21}M_{55}$ ($N = 1340$). More precisely, if we assume that the long period d_m varies with the degree of polymerization as $N^{2/3}$ due to chain stretching,[34] a block copolymer $S_{24}B_{21}M_{55}$ with $N = 1655$ would have a long period $d_m \cong 110$ nm. Indeed, the long period measured for many other SBM lamellar solutions prepared with a copolymer having a similar degree of polymerization is systematically larger than 100 nm. For instance a $S_{25}B_{28}M_{47}$ block copolymer with $N = 1805$ dissolved in chloroform ($\phi = 0.22$) forms lamellae with a long period of 122 nm.[31] In conclusion, the long period in $S_{11}B_{19}M_{70}$/toluene solutions seems to be too small by a factor 2.

In the literature, anomalous values of the long period of SBM morphologies are generally associated with the mixing of the S and M end blocks in S + M microdomains.[35–37] As already discussed in the Introduction, there is a fundamental difference between SBM block copolymers where the end blocks are phase-separated and their counterparts with mixed end blocks. The former behave like ABC copolymers while the latter behave very much like ABA copolymers. Accordingly, the long period of an ABA copolymer is about the half of that expected for ABC copolymer with the same molecular weight. Morphologies where S and M are mixed have already been observed in SBM and MSBSM[38] block copolymers. End blocks mix when at least one of them is short, which minimizes the enthalpy penalty,[37] as is the case for the $S_{11}B_{19}M_{70}$ block copolymer.

III.3. Lamellae Alignment under Shear Flow. Let us first determine the state of orientation at steady state of $S_{11}B_{19}M_{70}$/toluene solutions under steady shear. As stated earlier, it is important to notice that the order−disorder transition is not accessible so that we always start from an ordered phase. Figure 5 shows the two-dimensional scattering patterns observed at steady state in the $(\vec{q}_{\vec{V}}, \vec{q}_{\vec{\omega}})$ plane (radial observation) and in the $(\vec{q}_{\vec{\nabla V}}, \vec{q}_{\vec{\omega}})$ plane (tangential observation) for low, intermediate, and high shear rates ($C = 0.25$ g/g). *At low shear rates* ($\dot{\gamma} \cong 0.1$ s^{-1}), we observe intense meridian Bragg peaks centered at $\Phi = \pm 90°$ in both the radial and tangential planes. This indicates perpendicular orientation with the layers of the lamellae lying in the $(\vec{V}, \vec{\nabla V})$ plane, their normal being parallel to the vorticity direction (Figure 1a). *At high shear rates* ($\dot{\gamma} = 30$ s^{-1}), the state of orientation is totally different. In the radial plane, there is no diffracted intensity apart from two very weak meridian peaks. In the tangential plane, there are two intense equatorial peaks centered at $\Phi = 0°$ and $\Phi = 180°$. The absence of diffracted intensity in the radial plane and the presence of equatorial peaks in the tangential plane indicate a preference for obtaining lamellae in parallel orientation. The layers of the lamellae are parallel to the $(\vec{\nabla V}, \vec{\omega})$ plane, and their normal is along the velocity-gradient direction (Figure 1b). *At intermediate shear rate* ($\dot{\gamma} = 20$ s^{-1}), we detect meridian Bragg peaks in the radial plane and both meridional and equatorial peaks in the tangential plane. This is the signature of mixed orientation with coexistence of perpendicular and tangential alignments. This mixed orientation persists under shearing over very long periods of time without any drift of the system toward a preferential orientation.

These observations are rationalized in Figure 6a where we plot the intensity detected in the tangential plane at $\Phi = 90°$ and $\Phi = 180°$ against the shear rate. Stable perpendicular orientation ($I(90°) \gg I(180°)$) is observed over a wide range of shear rates ranging from the lowest experimentally accessible shear rate ($\dot{\gamma} \cong 0.01$ s^{-1}) to $\dot{\gamma} \cong 10$ s^{-1}. Perpendicular and parallel orientations coexist for $\dot{\gamma} = \dot{\gamma}_c \cong 20$ s^{-1}. Stable parallel orientation ($I(180°) \gg I(90°)$) is obtained in a narrow range of

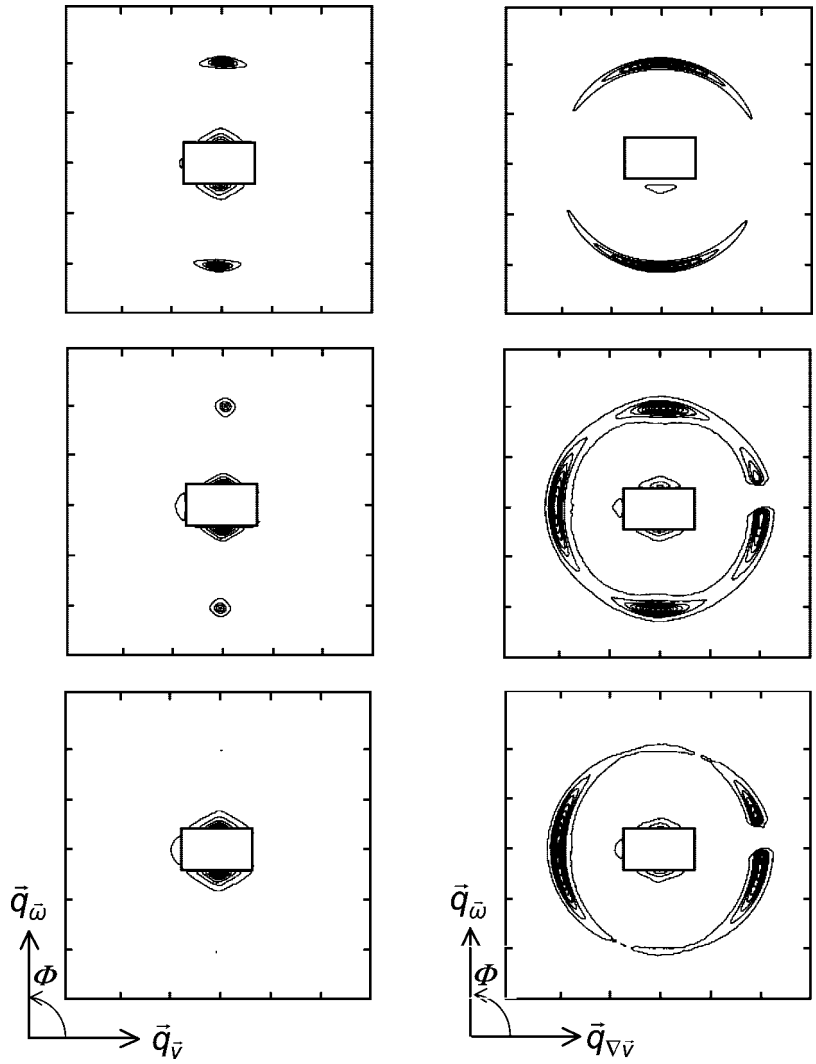

Figure 5. Two-dimensional scattering patterns scattered at different shear rates in the radial and tangential configurations from the $S_{11}B_{19}M_{70}$/toluene solution ($C = 0.25$ g/g). From top to bottom: $\dot{\gamma} = 0.1$ s^{-1}, $\dot{\gamma} = 20$ s^{-1}, and $\dot{\gamma} = 30$ s^{-1}. The intensity is plotted on a logarithm scale.

shear rates above $\dot{\gamma}_c$. When the shear rate is further increased ($\dot{\gamma} > 40$ s^{-1}), measurements become impossible because huge normal stresses develop in the shearing cell, which lead to the expulsion of the material out of the Couette cell.

To test the generality of this behavior, we have carried out the same analysis for the $S_{24}B_{21}M_{55}$/toluene solution (Figure 6b). According to the previous section, this copolymer forms lamellae with the middle block in a bridge conformation. Again, the orientation is predominantly perpendicular at low shear rates and parallel at high shear rates. Both orientations coexist in the vicinity of $\dot{\gamma}_c \cong 15$ s^{-1}.

III.4. Defects and Disorder. The azimuthal plots $I(\Phi)$ shown in Figure 7 present the variations of the scattered intensity with the azimuthal angle Φ. In this representation, the width of the diffraction peaks reflects the angular distribution of orientations in both the ($\vec{V}$, $\vec{\omega}$) plane (radial observation) and the ($\nabla\vec{V}$, $\vec{\omega}$) plane (tangential observation). The total intensity integrated over a diffraction peak is proportional to the volume fraction of the lamellae that satisfy the Bragg condition.

Let us first analyze the case of *perpendicular orientation at low shear rates* (Figure 7a,a′). Since the meridian peaks in the radial scattering pattern are remarkably sharp, we argue that the lamellae are well oriented along the $\vec{V}$ direction with a very narrow angular distribution. The peaks in the tangential scattering pattern are much broader. This shows that the planes containing the lamellae do not necessarily coincide with the ($\vec{V}$, $\nabla\vec{V}$) plane. Instead, they can be tilted with respect to the $\vec{V}$ direction. The normal to the lamellae is still in the ($\nabla\vec{V}$, $\vec{\omega}$) plane, but it makes an angle ($\vec{\omega}$, $\vec{n}$) with the vorticity direction (Figure 8a). This defect of orientation is responsible for a loss of scattered intensity in the radial direction because only those lamellae having a normal parallel to the beam contribute to the scattered intensity. We note that the total intensity detected in the tangential configuration ($I_t \cong 5 \times 10^5$) is nearly twice the intensity measured in the radial configuration ($I_t \cong 3 \times 10^5$). This confirms that the angle ($\vec{\omega}$, $\vec{n}$) can take a broad range of values. We have performed the same analysis when the shear rate is increased from 0.1 to 10 s^{-1}. The global orientation of the lamellae and the overall shape of the scattering peaks do not change dramatically. In the tangential plane, we note that the integrated intensity increases when the shear rate is increased from $\dot{\gamma} = 0.1$ s^{-1} to $\dot{\gamma} = 10$ s^{-1}, indicating that the alignment is somewhat perfected when the shear rate is increased.

Let us now turn our attention to the case of *parallel orientation at high shear rates* (Figure 7b,b′). For $\dot{\gamma} = 30$ s^{-1}, we detect some residual intensity in the radial plane due to the persistence of lamellar domains in the perpendicular orientation. The corresponding integrated intensity represents about 15% of the integrated intensity detected for perpendicular orientation at low shear rates. This shows that the parallel orientation is far from being perfect and that it coexists with a significant degree of perpendicular orientation. This is corroborated by a

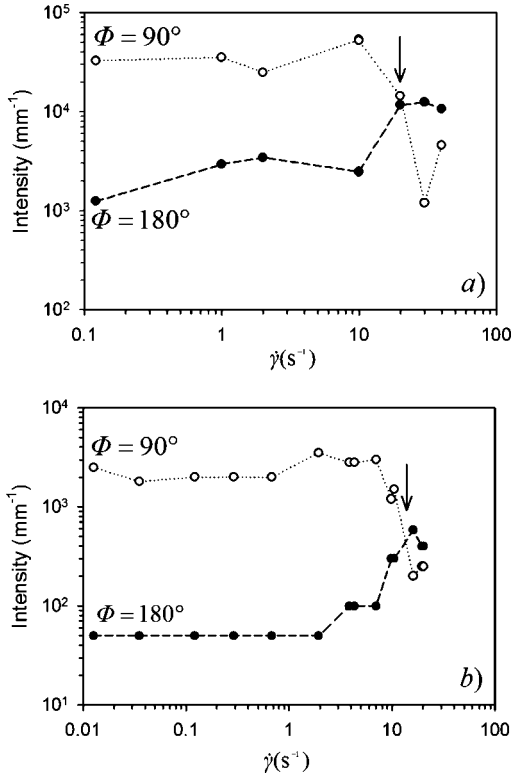

Figure 6. Maximum peak intensity vs shear rate in the tangential plane ($\vec{q}_{\nabla\vec{v}}$, $\vec{q}_{\vec{\omega}}$). (a) $S_{11}B_{19}M_{70}$/toluene solution ($C = 0.25$ g/g); (b) $S_{24}B_{21}M_{55}$/toluene solution ($C = 0.30$ g/g). Open symbols refer to the meridian peak situated at $\Phi = 90°$ and full symbols to the equatorial peak at $\Phi = 180°$). The lines are guides for the eye.

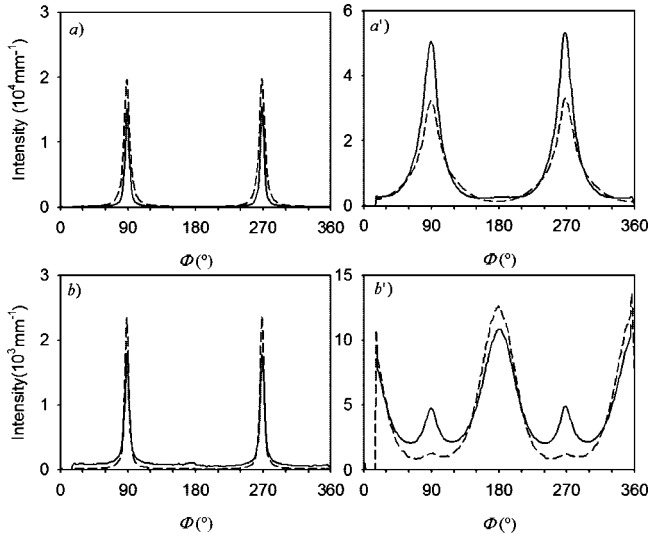

Figure 7. Azimuthal plots of the intensity vs the azimuthal angle in the radial plane ($\vec{q}_{\vec{v}}$, $\vec{q}_{\vec{\omega}}$) (graphs on the left-hand side) and in the tangential plane ($\vec{q}_{\nabla\vec{v}}$, $\vec{q}_{\vec{\omega}}$) (graphs on the right-hand side) for the $S_{11}B_{19}M_{70}$/toluene solution ($C = 0.25$ g/g). (a) and (a′): $\dot{\gamma} = 0.1$ s^{-1} (dashed line) and $\dot{\gamma} = 10$ s^{-1} (full line). (b) and (b′): $\dot{\gamma} = 30$ s^{-1} (dashed line) and $\dot{\gamma} = 40$ s^{-1} (full line).

close examination of the scattering patterns in the tangential plane, which exhibits small meridian peaks at $\Phi = 90°$ and 270°. The equatorial peaks at $\Phi = 0°$ and 180°, which originates from the diffraction by the lamellar domains in parallel orientation, are fairly broad. This shows that the lamellae are not perfectly parallel to the ($\vec{V}$, $\vec{\omega}$) plane and that they are tilted with respect to the $\vec{V}$ direction, their normal in the ($\nabla\vec{V}$, $\vec{\omega}$) plane being then inclined with respect to the vorticity direction

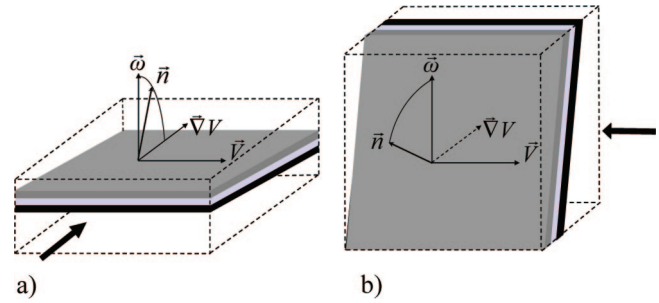

Figure 8. Schematic view of the dominant lamellar orientation at low (a) and high (b) shear rates in the ($\vec{V}$, $\vec{\omega}$) and ($\nabla\vec{V}$, $\vec{\omega}$) planes. The layers of the lamellae are perfectly oriented along the $\vec{V}$ direction, but they exhibit a fairly wide distribution of orientation in the ($\nabla\vec{V}$, $\vec{\omega}$) plane. The arrows indicate the direction of the X-ray beam.

(Figure 8b). We also note that the integrated intensity I_t is smaller than for the case of perpendicular orientation. This does not necessarily suggest a smaller degree of alignment since the number of lamellae satisfying the Bragg conditions is intrinsically limited by the curvature introduced by the Couette geometry. Experimentally, we have observed that the quality of alignment is worse when the shear rate is increased. At $\dot{\gamma} = 40$ s^{-1}, not only the fraction of lamellae in perpendicular orientation increases, but an isotropic background contribution appears. This suggests that the lamellar structure is destroyed by the flow leading to shear-induced disordered state.

III.5. Lamellae Alignment upon Flow Cessation. We now address the following issue: does the alignment persist upon flow cessation, or does it subsequently evolve toward a different state? To answer this question, we have compared the scattering patterns detected under flow and at rest upon flow cessation. For the perpendicular orientation obtained at low shear rates, the scattering patterns (not shown) remained unchanged even after the solution has been kept at rest for a long time ($\cong 10^3$ s). For the parallel orientation obtained at high shear rates, the scattering patterns evolved significantly after flow cessation. This is shown in Figure 9, where we compare the scattering profiles $I(\Phi)$ measured under flow and at rest for $\dot{\gamma} = 40$ s^{-1}. In the radial plane, the meridian peaks associated with perpendicular orientation decrease significantly whereas in the tangential plane the equatorial peaks due to parallel orientation become higher and sharper upon flow cessation. Moreover, the isotropic scattering contribution observed under flow disappears at rest, showing some reordering and reorientation of the fraction of material disordered by the flow. The scattering pattern in the radial plane reveals another noteworthy feature. Upon flow cessation, a peak grows at $\Phi = 180°$, suggesting that some fraction of lamellae is now in the "forbidden" transverse orientation. Still it is difficult to estimate the volume fraction of lamellae in transverse alignment from the integrated intensity because the scattered intensity only reflects those lamellae satisfying the Bragg conditions. In conclusion, the state of alignment obtained after shearing at high shear rates is complex, with a coexistence of lamellae in parallel, perpendicular, and transverse orientations.

III.6. Reversibility of the Flip of Orientation. Remarkably, the flip of orientation between perpendicular and parallel alignments that occurs when the shear rate is increased above $\dot{\gamma}_c$ is reversible: starting from a predominantly parallel alignment just above $\dot{\gamma}_c$, the initial perpendicular orientation is recovered when the shear rate is lowered below $\dot{\gamma}_c$. The value of $\dot{\gamma}_c$ is independent of whether the transition is approached from above or below. However, the time scales involved and the underlying mechanisms appear to be notably different. This is shown in Figures 10a,b where we plot the time variations of the maximum

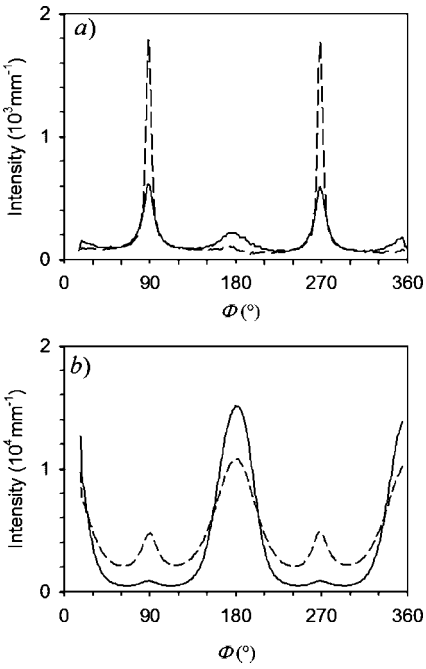

Figure 9. Azimuthal plots of the intensity scattered under shear (dashed lines) and upon flow cessation (continuous lines), in the radial plane ($\vec{q}_{\nabla}$, $\vec{q}_{\vec{\omega}}$) (a) and in the tangential plane ($\vec{q}_{\nabla\nabla}$, $\vec{q}_{\vec{\omega}}$) (b). The solution is the $S_{11}B_{19}M_{70}$/toluene solution ($C = 0.25$ g/g). The shear rate is $\dot{\gamma} = 40$ s^{-1}.

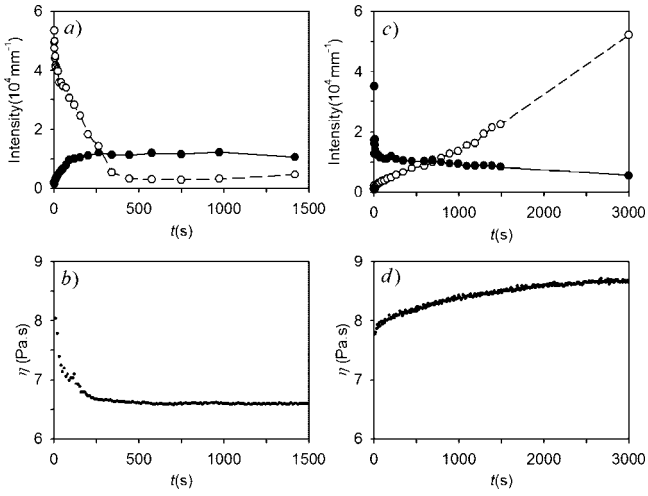

Figure 10. Transient behaviour of the maximum peak intensity at $\Phi = 90°$ (○) and $\Phi = 180°$ (●) (tangential plane) and of the viscosity when the shear rate is increased from 0.1 to 40 s^{-1} (a, b) and decreased from 30 to 10 s^{-1} (c, d). The lines are guides for the eye. The data are for the $S_{11}B_{19}M_{70}$/toluene solution ($C = 0.25$ g/g).

intensity in the meridian peak ($\Phi = 90°$) and in the equatorial peak ($\Phi = 180°$) (both measured in the tangential plane) and of the viscosity, when the shear rate is quenched from low $\dot{\gamma} \cong 0.1$ s^{-1}) to high values ($\dot{\gamma} \cong 40$ s^{-1}) and reversely from high ($\dot{\gamma} \cong 30$ s^{-1}) to low ($\dot{\gamma} \cong 0.1$ s^{-1}) values. In the former experiment, we observe that the growth of the parallel alignment and the disappearance of the perpendicular alignment occur concomitantly. The orientation is predominantly parallel after only 300 s. These variations of the scattered intensity and of the viscosity suggest that the transition from perpendicular to parallel orientation proceeds by a rotation of the lamellae from the initial perpendicular alignment to the preferred parallel alignment. The rotation of the lamellae is associated with a decrease of the viscosity that reaches a plateau when the orientation has become predominantly parallel. At longer times, the meridian intensity

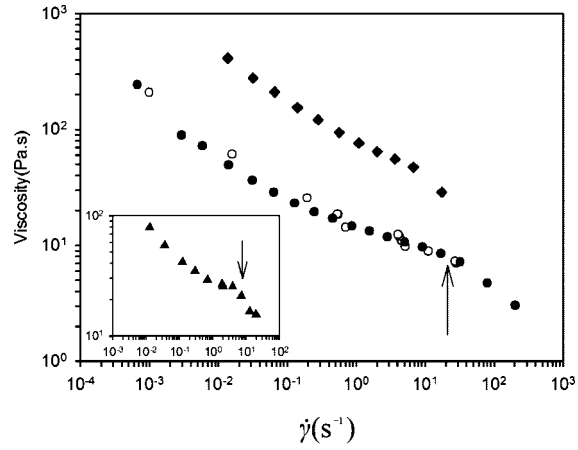

Figure 11. Flow curves of $S_{11}B_{19}M_{70}$/toluene solutions (●, ○: $C = 0.25$ g/g; ♦: $C = 0.30$ g/g) and of a $S_{24}B_{21}M_{55}$/toluene solution (inset, $C = 0.30$ g/g). Open and full symbols refer to in-situ rheology measurements and to off-line measurements, respectively. The arrows indicate the shear rate where parallel and perpendicular alignments coexist.

increases again while the equatorial intensity decreases, which indicates that the parallel alignment is progressively destroyed by the flow as it has been discussed in the previous section. The time variations of the scattered intensities and of the viscosity are completely different when we start from a predominantly parallel orientation and we lower the shear rate below $\dot{\gamma}_c$ (Figure 10c,d). Clearly, the intensity in the equatorial peak instantaneously drops to its final value while that in the meridian peak grows very slowly. Only after several thousands of seconds its reaches a value close to that measured at steady state for this particular shear rate. This strongly suggests that the lamellae are first destroyed and that subsequently re-form in the expected perpendicular orientation. The buildup of the structure is followed by a gradual increase of the viscosity. In conclusion, even though the flip of orientation around $\dot{\gamma}_c$ is reversible, it follows two different mechanisms: rotation of the lamellae (perpendicular → parallel) or melting and buildup of lamellae (parallel → perpendicular).

III.7. Bulk Rheology. In order to characterize more thoroughly the importance of the microstructure, we have conducted a series of rheological measurements using both cone and plate and Couette geometry. Figure 11 depicts the variations of the steady-state viscosity vs the shear rate for different SBM solutions. All the curves exhibit the same characteristic shape. In the domain where perpendicular alignment is dominant, the viscosity smoothly decreases as the shear rate is increased. Interestingly, we note the absence of Newtonian plateau at the lowest shear rates, indicating the presence of long relaxation times. The decrease of the viscosity becomes slower as the shear rate approaches the value $\dot{\gamma}_c$ at which perpendicular and parallel orientations coexist. Above $\dot{\gamma}_c$ shear thinning becomes more pronounced. The coexistence is associated with the existence of a kink point on the flow curve. At very high shear rates, the solutions are expelled from the geometry, preventing measurements in this shear regime. For the highest concentration ($C = 0.3$ g/g) investigated, this happens near $\dot{\gamma}_c$, so that stable parallel alignment is never observed.

IV. Discussion

IV.1. Characteristic Features of the Shear-Flow Alignment of Lamellar SBM Solutions. The existence of two dominant states of orientation and the possibility to induce a flip of orientation from perpendicular to parallel are globally consistent with the results reported for diblock solutions subjected to steady shear flows.[1,17–20] Despite this apparent

similarity, however, there are fundamental differences that need further attention. First, while in diblock solutions the parallel orientation is generally preferred once it is reached for both oscillatory and steady flow;[17,18,20] in SBM triblocks we have found that the lamellae switch reversibly between the parallel and perpendicular orientations when the shear rate is increased or lowered above or below a well-defined value $\dot{\gamma}_c$. At shear rates comparable to $\dot{\gamma}_c$, we have observed the development of a complex mixed orientation state characterized by a long-lived coexistence of parallel and perpendicular orientations.

IV.2. Microscopic Mechanisms at the Origin of Perpendicular and Parallel Alignments. The value of the shear rate $\dot{\gamma}_c$ where the alignment flips reversibly between the perpendicular and parallel orientations is of the order of the inverse of the relaxation time of individual chains, which has been determined by independent viscoelasticity measurements. This shows that single chain dynamics plays an important role in the selection of a particular state of orientation. The importance of chain conformational distortions in the development of destruction of lamellae with a particular orientation has been identified and discussed in detail for the case of diblock copolymers subjected to oscillatory shearing.[11] The same kind of arguments can be applied to our triblock copolymer solutions. At low shear rates ($\dot{\gamma}\tau < 1$), the lamellae adopt perpendicular orientation because they have time to relax the deformation they experience in the flow; they move freely in their layers, and they are insensitive to vorticity effects. At high shear rates ($\dot{\gamma}\tau > 1$), the chains are strongly stretched and oriented by the flow; the perpendicular orientation is no longer stable, and the lamellae switch to parallel alignment. This orientation is favorable because the layers of the microstructure can slide relative to each other, thus reducing the conformational distortions of the chains. This argument is general, and it should apply whenever the chain architecture permits the relative sliding of the layers. It has been used to explain the parallel orientation observed in diblock lamellae.[1,3,12,14] In pentablock copolymers where the different layers are mechanically coupled, relative sliding of the layers is not possible, and parallel alignment is never observed.[24]

In general, the relative sliding of lamellae in the parallel orientation must occur through narrow interpretation zones between polymer-like brushes forming the microdomains. These zones contribute to transmit stress across the lamellae. For the case of (diblock) melts, it has been predicted theoretically[39] and shown experimentally[40] that the lamellae contract to resist the entropic penalty associating with chain stretching. Such an effect is not seen in our experiments where the lamellae spacing keep its quiescent value within the experimental accuracy. It is not sufficient however to have easy sliding of the layers to ensure the stability of the parallel orientation. Real experiments involve the presence of shearing surfaces that confine the material. While the perpendicular orientation is relatively insensitive to the presence of shearing surfaces, the parallel orientation does not accommodate easily the small gap variations that are associated with unavoidable mechanical imperfections of the Couette cell. The number of layers must vary to remain commensurate with the gap thickness. This generates defects and compressive stress that contribute to destabilize the parallel orientation. We speculate that this effect can be at the origin of the shear-induced disordering of the lamellae that is observed at high shear rates. In that respect the occurrence and the quality of the parallel alignment do depend on the type of solicitation (oscillatory or permanent flow), on the strain amplitude, on the geometry (Couette or cone and plane), and on the mechanical quality of the shearing cell. Interestingly, we have observed that normal stress effects and sample expulsion are less critical in cone and plate geometry, allowing us to perform rheological measurements at higher shear rates than in Couette geometry. The same effect could explain the absence of return to parallel orientation at very low shear rates.

IV.3. Stability of the Perpendicular and Parallel Orientations. Even though the perpendicular and parallel orientations are dominant at low and high shear rates, respectively, both alignment states are affected by the presence of defects. The perfection of the perpendicular alignment is significantly greater than that of the parallel orientation. *In the perpendicular orientation*, the layers of the lamellae are always perfectly aligned with the velocity direction, but their normal, which lies in the velocity gradient−vorticity plane, exhibits a fairly wide angular distribution around the vorticity direction. This can be explained by a shear-induced undulation instability of the lamellae along the velocity-gradient direction or to the persistence of a multigrain structure stabilized by specific defects. Undulation of lamellae has already been reported for the case of lamellar diblock solutions exhibiting perpendicular orientation.[18] This was accompanied by a progressive destruction of the perpendicular alignment, which is not seen here in triblock solutions. *In the parallel orientation*, the lamellae also undulate, but now the undulations are along the vorticity direction. More importantly, a significant amount of lamellae in the perpendicular orientation coexists with the dominant parallel alignment. Increasing the shear rate does not improve the quality of the parallel orientation but instead provokes a shear-induced disordering of the lamellae, even at a moderate shear rate. The disordering of the lamellae is associated with the appearance of large normal stress effects leading to the expulsion of the solution out of the Couette geometry. This considerably reduces the range of shear rates where a stable parallel (though imperfect) alignment state can be obtained.

IV.4. Origin of the Transverse Orientation. For diblock copolymer melts, transverse orientation, which does not preserve the long period, is generally associated with transient states[5–7] or with the presence of specific kink bands defects that act to stabilize it.[9] On the other hand, it has been argued that a bimodal parallel-transverse texture constitutes a route to parallel alignment at high frequencies because chains in either the transverse or parallel alignment are not reoriented by the shear deformation.[11] In our experiments, the transverse orientation appears upon flow cessation. The fraction of disordered material associated with shear disordering disappears, and simultaneously a small amount of lamellae in transverse orientation is detected. Recently, stable transverse orientation has been observed in pentablock copolymer melts upon flow cessation[24] and during solution extrusion[29] under particular conditions. The existence of transverse orientation relies on the existence of chains that are strongly extended and aligned by the strong flow and that template the growth of microdomains in transverse orientation. The same mechanism must operate here for the case of SBM copolymer solutions.

V. Concluding Remarks

The results of this study highlight the specificity of the behavior of ABC copolymer lamellar mesophases subjected to steady shear flow with respect to other block copolymer mesophases. The application of steady flow induces the alignment of the lamellae along the perpendicular or parallel directions depending on the shear rate intensity. The orientation flips reversibly from one orientation to another when the shear rates is increased or decreased above a characteristic frequency ω_C given by the inverse of the single chain relaxation time. A higher degree of ordering is reached for the perpendicular than for the parallel orientation, where mesophases are progressively destroyed when the shear rate is increased well above ω_C. This

behavior is intermediate between that of diblocks, where the parallel orientation seems to be favored, and that of pentablocks, where the parallel orientation is not observed. Finally, it is interesting to note that all these results have been obtained for triblock solutions where long-lived transient states are absent.

Acknowledgment. The authors thank Arkema for providing the block copolymers used in this study, in particular Dr. C. Navarro. We are indebted to Fabrice Monti for his help in the experiments. We thank Ludwik Leibler for his enthusiastic support and stimulating discussions. We are grateful to Dr. T. Narayanan for generous support at ESRF and J. Gorini and L. Goirand for the aluminum cell design. We are indebted to ESRF for beam time allocation.

References and Notes

(1) Koppi, K. A.; Tirrell, M.; Bates, F. S.; Almdal, K.; Colby, R. H. *J. Phys. II* **1992**, *2*, 1941–1959.
(2) Winey, K. A.; Patel, S. S.; Larson, R. G.; Watanabe, H. *Macromolecules* **1993**, *26*, 4373–4375.
(3) Patel, S. S.; Larson, R. G.; Winey, K. I.; Watanabe, H. *Macromolecules* **1995**, *28*, 4313–4318.
(4) (a) Zhang, Y.; Wiesner, U.; Spiess, H. W. *Macromolecules* **1995**, *28*, 778–781. (b) Wiesner, U. *Macromol. Chem. Phys.* **1997**, *198*, 3319–3352.
(5) (a) Gupta, V. K.; Krishnamoorti, R.; Chen, Z.-R.; Kornfield, J. A.; Smith, S. D.; Satkowski, M. M.; Grothaus, J. T. *Macromolecules* **1996**, *29*, 875–884. (b) Chen, Z.-R.; Issaian, A. M.; Kornfield, J. A.; Smith, S. D.; Grothaus, J. T.; Satkowski, M. M. *Macromolecules* **1997**, *30*, 7096–7114. (c) Chen, Z. R.; Kornfield, J. A. *Polymer* **1998**, *39*, 4679–4699.
(6) Okamoto, S.; Saijo, K.; Hashimoto, T. *Macromolecules* **1994**, *27*, 5547–5555.
(7) Pinheiro, B. S.; Hajduk, D. A.; Gruner, S. M.; Winey, K. I. *Macromolecules* **1996**, *29*, 1482–1489.
(8) Polis, D. L.; Winey, K. I. *Macromolecules* **1996**, *29*, 8180–8187.
(9) Polis, D. L.; Winey, K. I. *Macromolecules* **1998**, *31*, 3617–3625.
(10) Zhang, Y.; Wiesner, U. *J. Chem. Phys.* **1995**, *103*, 4784–4793.
(11) Chen, Z.-R.; Kornfield, J.; Smith, S. D.; Grothaus, J. T.; Satkowski, M. M. *Science* **1997**, *277*, 1248–1253.
(12) Fredrickson, G. H. *J. Rheol.* **1994**, *38*, 1045–1067.
(13) Zhang, Y.; Wiesner, U.; Yang, Y.; Pakula, T.; Spiess, H. W. *Macromolecules* **1996**, *29*, 5427–5431.
(14) Riise, B. L.; Fredrikson, G. H.; Larson, R. G.; Pearson, D. S. *Macromolecules* **1995**, *28*, 7653–7659.
(15) Gupta, V. K.; Krishnamoorti, R.; Kornfield, J. A.; Smith, S. D. *Macromolecules* **1996**, *29*, 1359–1362.
(16) Maring, D.; Wiesner, U. *Macromolecules* **1997**, *30*, 660–662.
(17) Balsara, N. P.; Hammouda, B.; Kesani, P. K.; Jonnalagadda, S. V.; Straty, G. C. *Macromolecules* **1994**, *27*, 2566–2573.
(18) Wang, H.; Kesani, P. K.; Balsara, N. P.; Hammouda, B. *Macromolecules* **1997**, *30*, 982–992.
(19) Wang, H.; Newstein, M. C.; Krishnan, A.; Balsara, N. P.; Garetz, B. A.; Hammouda, B.; Krishnamoorti, R. *Macromolecules* **1999**, *32*, 3695–3711.
(20) Zryd, J. L.; Burghardt, W. R. *Macromolecules* **1998**, *31*, 3656–3670.
(21) Tepe, T.; Hadjuk, D. A.; Hillmyer, M. A.; Weimann, P. A.; Tirrell, M.; Bates, F. S. *J. Rheol.* **1997**, *41*, 1147–1171.
(22) Hermel, T. J.; Wu, L.; Hahn, S. F.; Lodge, T. P.; Bates, F. S. *Macromolecules* **2002**, *35*, 4685–4689.
(23) Stangler, S.; Abetz, V. *Rheol. Acta* **2003**, *42*, 569–577.
(24) Vigild, M. E.; Chu, C.; Sugiyama, M.; Chaffin, K. A.; Bates, F. S. *Macromolecules* **2001**, *34*, 951–964.
(25) (a) Wu, L.; Lodge, T. P.; Bates, F. S. *Macromolecules* **2004**, *37*, 8184–8187. (b) Wu, L.; Lodge, T. P.; Bates, F. S. *Macromolecules* **2006**, *39*, 294–299.
(26) (a) Villar, M. A.; Rueda, D. R.; Ania, F.; Thomas, E. L. *Polymer* **2002**, *43*, 5139–5145. (b) Ha, Y. H.; Thomas, E. L. *Macromolecules* **2002**, *35*, 4419–4428.
(27) Leist, H.; Geiger, K.; Wiesner, U. *Macromolecules* **1999**, *22*, 1315–1317.
(28) Carreras, E. S.; Piau, J.-M.; El Kissi, N.; Pignon, F.; Panine, P. *J. Rheol.* **2006**, *50*, 803–1023.
(29) Harada, T.; Bates, F. S.; Lodge, T. P. *Macromolecules* **2003**, *36*, 5440–5442.
(30) Navarro, C.; Marcarian, X.; Vuillemin, B. *Macromol. Symp.* **1998**, *132*, 263–269.
(31) Fleury, C. Doctoral Thesis, Université Pierre et Marie Curie, **2001**.
(32) Narayanan, T.; Diat, O.; Boesecke, P. *Nucl. Instrum. Methods Phys. Res.* **2001**, *A467−568*, 1005–1009.
(33) Rubinstein, M.; Obukhov, S. P. *Macromolecules* **1993**, *26*, 1740–1750.
(34) Stadler, R.; Auschra, C.; Beckmann, J.; Krappe, U.; Voigt-Martin, I.; Leibler, L. *Macromolecules* **1995**, *28*, 3080–3091.
(35) Brinkmann-Rengel, S.; Abetz, V.; Stadler, R.; Thomas, E. L. *Kautsch. Gummi Kunstst.* **1999**, *12*, 806–813.
(36) Corté, L.; Yamauchi, K.; Court, F.; Cloitre, M.; Hashimito, T.; Leibler, L. *Macromolecules* **2003**, *36*, 7995–7706.
(37) Yamaguchi, D.; Cloitre, M.; Panine, P.; Leibler, L. *Macromolecules* **2005**, *38*, 7798–7806.
(38) Yu, J. M.; Dubois, Ph.; Jérôme, R. *Macromolecules* **1997**, *30*, 4984–49.
(39) Williams, D. R. M.; Mackintosh, F. C. *Macromolecules* **1994**, *27*, 7677–7680.
(40) (a) Polis, D. L.; Winey, K. I.; Ryan, A. J.; Smith, S. D. *Phys. Rev. Lett.* **1999**, *83*, 2861–2964. (b) Qiao, L.; Ryan, A. J.; Winey, K. I. *Macromolecules* **2002**, *35*, 3596–3600.

MA702876K